Interpretation of the Electronic Spectra of the Confacial Bioctahedral Nonahalides [Ru₂Cl₉]³⁻ and [Ru₂Br₉]³⁻ using the SCF-Xα-SW Method: Location of the σ ⟶ σ* Transition†

Graham A. Heath and John E. McGrady
Research School of Chemistry, The Australia National University, Canberra, ACT 0200, Australia

Considerable progress has been made in assigning the UV/VIS/near-IR electronic spectra (5000–50 000 cm⁻¹) of [Ru₂Cl₉]³⁻ and [Ru₂Br₉]³⁻, with the aid of SCF-Xα-SW calculations. A conceptual framework within which band energies and relative intensities can be discussed was constructed by reference to the corresponding [MX₆]ⁿ⁻ monomers. First, an empirical correction ($\delta_{c.t.}$) of 7500 cm⁻¹ has been established for Xα-computed energies of frankly charge-transfer (c.t.) transitions, based on the discovery that the calculated X→M charge-transfer (x.m.c.t.) transitions are faithfully linearly correlated (unity gradient) with observed band energies for the congeneric t_{2g}^5 complexes [RuCl₆]³⁻, [RuBr₆]³⁻, [IrCl₆]²⁻, and [IrBr₆]²⁻. Secondly, the calculated oscillator strengths for c.t. transitions of monomeric hexahalides successfully model observed band intensities, and can be understood in terms of the mutual overlap of ligand-based components of the donor and acceptor orbitals. For binuclear [Ru₂Cl₉]³⁻ and [Ru₂Br₉]³⁻ the intense absorption bands above 30 000 cm⁻¹ are readily assigned to x.m.c.t. transitions to the {7e″, 9e′} levels, derived from the single-ion e_g orbitals. In contrast, the anticipated c.t. to the t_{2g}-derived levels (*i.e.* to unfilled 5a₂″) loses intensity in the trigonal field of the confacial complexes, and the prominent near-UV/VIS features are assigned instead to transitions within the metal–metal orbital manifold. In particular, the binuclear σ ⟶ σ* transition is located at 22 500 cm⁻¹ for [Ru₂Cl₉]³⁻ and 20 000 cm⁻¹ for [Ru₂Br₉]³⁻, well above the calculated values. The discrepancy between observed and calculated σ ⟶ σ* transition energies arises through the neglect of electron-correlation effects in the Xα calculations. The implied value of the two-electron exchange term *K* is about 7800 cm⁻¹ for both complexes. Thus, two major empirical adjustments ($\delta_{c.t.}$ and *K*) are required in the present analysis due to the limitations of the Xα method, and the status of these measures is examined.

Confacial bioctahedral complexes of [M₂X₉]ⁿ⁻ stoichiometry have a central position in transition-metal halide chemistry.[1] Compounds of this type containing the later heavy metals Os, Ir and Pt proved relatively elusive, but the recently reported crystal structures [2–4] of salts of [Os₂Br₉]³⁻, [Ir₂Cl₉]³⁻ and [Pt₂Br₉]⁻ illustrate that this chemistry is under current expansion. The sequence of structurally characterised confacial bioctahedral complexes containing 4d and 5d metals now spans Nb, Ta, Mo, W, Re, Ru and Rh,[5] as well as the aforementioned Os, Ir and Pt. The discovery and spectroelectrochemical characterisation of redox-related odd-electron states, commencing with the observation[6] of [Ru₂X₉]⁻¹²⁻/³⁻/⁴⁻, and now including[7–9] [Re₂X₉]⁻¹²⁻/³⁻, [Os₂X₉]⁻¹²⁻/³⁻ and [Ir₂X₉]⁻¹²⁻/³⁻ (X = Cl or Br), has greatly enlarged the number and variety of available complexes. This development opens up fundamental questions about the variation in metal–metal bonding across the series as a joint function of atomic number and oxidation state. Complexes with {d³d³} single-ion configurations ([Mo₂X₉]³⁻, [W₂X₉]³⁻, [Re₂X₉]⁻) contain a formal metal–metal triple bond, and have received long-standing attention in the literature.[10] In contrast, {d⁴d⁴} systems were unrepresented[11] until electrogeneration of [Re₂X₉]³⁻ and the isolation of [Os₂X₉]⁻ salts.[7,8] Equally however, {d⁵d⁵} systems such as [Ru₂X₉]³⁻ (the subject of this paper) and newly discovered[2,9] [Os₂X₉]³⁻ and [Ir₂X₉]⁻ are of interest in their own right because the bonding is purely σ in overall character and the maximum bond order is one.

The optical spectra (5000–50 000 cm⁻¹) of the whole family of confacial bioctahedral complexes should provide a wealth of electronic structural information but a consistent interpretation has yet to emerge, even for the major features. Bursten *et al.*[12] performed SCF-Xα-SW calculations on [Ru₂Cl₉]³⁻, and discussed the limited solid-state spectral information available to them largely in terms of transitions within the binuclear manifold of metal-based orbitals. In contrast, Seddon and co-workers,[5i] though using the molecular-orbital scheme constructed by Bursten, assigned the solution spectrum of [Ru₂Br₉]³⁻ solely in terms of charge-transfer transitions. Obviously, the true nature of the observed absorption bands merits clarification. The increasing body of related structural and spectroscopic data in our laboratory prompted us to undertake new, comparative calculations of the electronic structures of [Ru₂Cl₉]³⁻ and [Ru₂Br₉]³⁻, in both ground and excited states, and to extend these calculations for the first time to explicit evaluation of transition oscillator strengths. A satisfactory reconciliation of theory and observation has finally emerged, as described below.

Any cogent interpretation of the electronic spectra of these bioctahedra based on molecular-orbital calculations must take into account the intrinsic limitations of the computational method. The SCF-Xα-SW approach has been used with some success to describe the bonding and electronic spectra of a broad range of tansition-metal compounds,[13] and in particular has been shown to give an accurate estimate of the ligand-field splitting.[14] The description of ligand-to-metal charge-transfer (l.m.c.t.) transitions is considerably less realistic, in absolute terms,[13,15] with promotion energies for simple monomeric systems being underestimated by as much as 8000 cm⁻¹. This arises through the intrinsic tendency of conventional Xα methods to exaggerate d-electron stability. Solomon and co-workers[16] advocated calibrating the wavefunction by varying

the sphere radii until (*i*) the ground-state *g* tensor satisfies the experimentally determined values, and (*ii*) the potentials are matched at common sphere boundaries. This promising procedure results in improved l.m.c.t. energies for paramagnetic systems, so long as measured *g* values are accessible, although the matching of potentials at sphere boundaries becomes increasingly difficult as the number of symmetry-distinct atoms in a molecule increases. The present $\{d^5d^5\}$ compounds, however, have $S = 0$ ground states.

An alternative strategy, which we explore in this work, is to establish an empirical correction factor for calculated charge-transfer energies. While this falls short of an absolute 'first principles' approach, it allows us to assign the spectra of complex $[M_2X_9]^{z-}$ systems by incorporating a fixed correction derived independently from fully documented c.t. spectra of simpler systems. Hexahalogenometalate complexes, $[MX_6]^{z-}$, have electronic spectra which are dominated by intense X→M charge-transfer (x.m.c.t.) bands, and these have been fully assigned in many cases.[17] As demonstrated below, the observed and calculated transition energies for these well understood octahedral monomers prove to be faithfully linearly related, which means that a simple, large but constant, correction is applicable to Xα-calculated x.m.c.t. transition energies. We have also found that the relative intensities of these transitions in $[MX_6]^{z-}$ complexes are well modelled by the computed oscillator strengths. Moreover, these oscillator-strength values can be understood by close examination of the composition and orientation of the donor and acceptor molecular orbitals. In the case of $[M_2X_9]^{z-}$ systems interpretation of the x.m.c.t. spectra is necessarily complicated by the profound reorganisation (trigonal perturbation) of the metal-based acceptor orbitals and by the presence of distinct bridging and terminal halide arrays (X_b and X_t), both of which can act as donors in charge-transfer excitation. Nevertheless, it has proved possible to resolve these complexities in x.m.c.t. assignment in the nonahalides by the two strategies outlined above, *i.e.* by application of an empirical frequency correction derived from the related monomers and by detailed consideration of the computed oscillator strengths.

Apart from x.m.c.t. transitions (and more directly connected with the question of metal–metal bonding), the interaction of the two adjacent low-spin d^5 centres gives rise to electronic transitions within the manifold formally derived from the octahedral t_{2g} orbitals, and also to transitions connecting the t_{2g}- and e_g-derived manifolds. This is shown schematically in Fig. 1, where the $[M_2X_9]^{3-}$ levels are classified according to their symmetry with respect to the M–M axis. Arrows indicate the only optically allowed transitions within the lower manifold, together with a favoured higher promotion.

A notable general problem exists in describing the excitation of weakly coupled electrons within the framework of molecular-orbital theory.[18] The $\{d^5d^5\}$ core of $[Ru_2X_9]^{3-}$ presents such a case. The energies of transitions involving the unpairing of these electrons tend to be severely underestimated by Xα calculations through neglect of two-electron repulsion terms and of configuration interaction (CI) which stabilises the ground state. For excitation within the t_{2g} manifold, when metal–metal bonding is weak these contributions can be of the same magnitude as the orbital separation.[18b] This has the disconcerting effect that the experimental band energy cannot be safely equated, even approximately, to the difference in the molecular-orbital energy levels connected by the transition, even when these levels are precisely located. The second category of excitation, connecting the t_{2g}- and e_g-derived manifolds of Fig. 1, is formally related to the underlying single-ion ligand-field separation. These transitions are relatively free of both charge-transfer and electron-correlation terms and should be computed accurately, as in the parent monomers.

In the present work, through exhaustive comparison of the observed and calculated spectra in the range 5000–50 000 cm⁻¹, we find that it is possible to assign the charge-transfer bands of
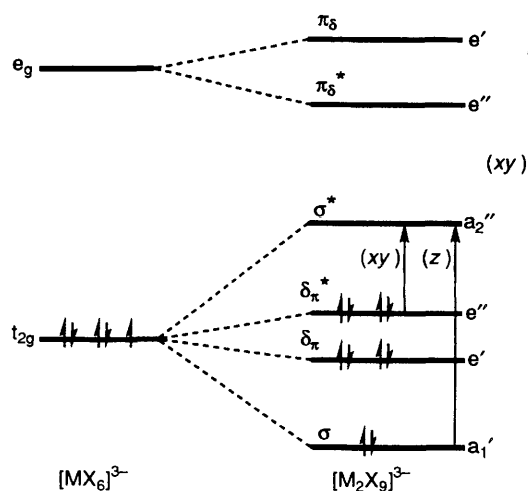
Fig. 1 Splitting of d^5 single-ion t_{2g} and e_g orbitals in the confacial bioctahedron

$[Ru_2X_9]^{3-}$ and, having recognised and eliminated these, to go on to identify the bands due to transitions between metal-based orbitals. We conclude that the important σ ⟶ σ* transition is located near 22 500 cm⁻¹ for $[Ru_2Cl_9]^{3-}$ and near 20 000 cm⁻¹ for $[Ru_2Br_9]^{3-}$, though the computed orbital separation is only 12 300 or 9400 cm⁻¹, respectively. In consequence, the contribution of electron-correlation effects to the observed transition energy is quantified as approximately 10 000 cm⁻¹ in both systems. Overall, these wide-ranging assignments embody two substantial adjustments to the Xα transition energies, and the basis for these empirical corrections is presented below for critical evaluation.

Methodology

Calculations were performed using standard versions of SCF-Xα-SW.[19] Atomic coordinates were generated from the corresponding crystal structures, idealised to O_h or D_{3h} symmetry for octahedra or confacial bioctahedra respectively. In order to calculate the correction factor for charge-transfer transition energies it is vital to ensure that the sphere radii are selected in a consistent manner. In all cases considered here the initial potential was generated from a superposition of neutral atomic potentials, and the sphere radii were taken as 89% of the atomic number radii. Structural parameters and sphere radii are summarised in Table 1.[20–23] A Watson sphere[24] of charge opposite to that of the complex ion (*i.e.* 3+ for $[RuX_6]^{3-}$ and $[Ru_2X_9]^{3-}$, 2+ for $[IrX_6]^{2-}$) was placed at the outer sphere boundary. The atomic exchange parameters were taken from the tabulations of Schwarz.[25] The wavefunction was expanded using spherical harmonics up to L = 4 on Ru or Ir, 3 on Cl or Br and 5 on the outer sphere. Core levels [Ru 1s,2s,2p,-3s,3p,3d,4s,4p; Ir (Ru),4d,4f,5s,5p; Cl 1s,2s,2p; Br (Cl),3s,3p,-3d] were confined to the atomic sphere in question and calculated explicitly at each iteration. The potential was considered converged when the change in potential was less than 10⁻⁵ Ry. Where orbital plots are given, successive contours are 0.001, 0.002, 0.004, 0.008, 0.02, 0.04, 0.08 and 0.2 (electron a_0^{-3})^½ (Figs. 8–10). In each case the orbital topology is defined by an accompanying perspective diagram. Slater-type calculations[26] were performed to obtain transition energies. Oscillator-strength values, *f*, were calculated according to the procedure devised by Noodleman.[27]

Results

(*a*) *Ground-state Electronic Structure.*—The energies and compositions of the molecular orbitals of $[RuCl_6]^{3-}$, $[RuBr_6]^{3-}$, $[Ru_2Cl_9]^{3-}$ and $[Ru_2Br_9]^{3-}$ are available as SUP 57043,

Table 1 Input geometric data for Xα calculations

Complex	Bond length/Å	Bond angle/°	Radii/Å
[RuCl₆]³⁻ (ref. 20)	Ru–Cl 2.369	90	Ru 2.5167 Cl 2.6802 7.1570*
[RuBr₆]³⁻ (ref. 21)	Ru–Br 2.514	90	Ru 2.5697 Br 2.9268 7.6776*
[IrCl₆]² (ref. 22)	Ir–Cl 2.31	90	Ru 2.4181 Cl 2.5975 6.9628*
[IrBr₆]²⁻ (ref. 23)	Ir–Br 2.52	90	Ru 2.5268 Br 2.9066 7.6687*
[Ru₂Cl₉]³⁻ [ref. 5(h)]	Ru–Ru 2.725 Ru–Clₜ 2.332 Ru–Cl_b 2.391	Ru–Ru–Clₜ 125	Ru 2.4850 Cl_b 2.5299 Clₜ 2.6468 8.8981*
[Ru₂Br₉]³⁻ [ref. 5(i)]	Ru–Ru 2.880 Ru–Brₜ 2.507 Ru–Br_b 2.510	Ru–Ru–Brₜ 125	Ru2.5459 Clₜ 2.9192 Cl_b 2.7487 9.6015*

* Radius of the outer sphere.
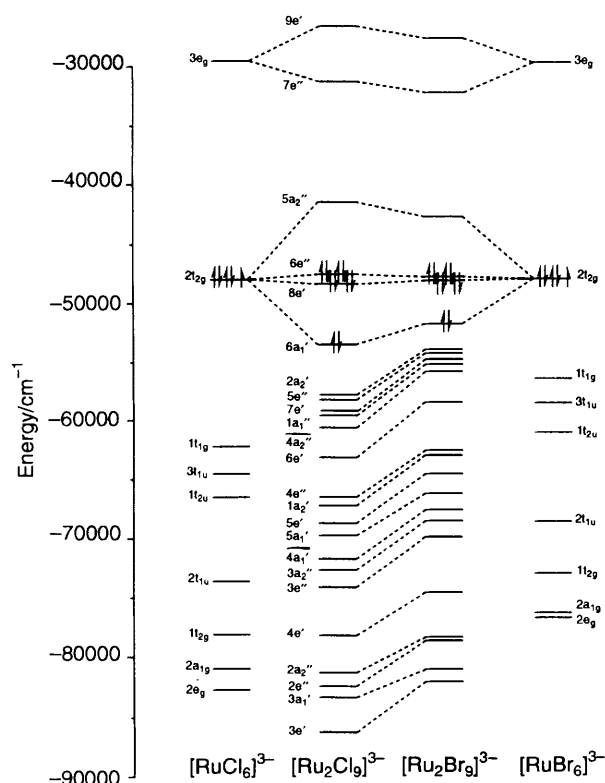
Fig. 2 Comparative molecular-orbital diagrams for [RuCl₆]³⁻, [Ru₂Cl₉]³⁻, [Ru₂Br₉]³⁻ and [RuBr₆]³⁻

as are data for [IrCl₆]²⁻ and [IrBr₆]²⁻. Fig. 2 shows a comparative molecular-orbital diagram for the four ruthenates. The numerical results for [Ru₂Cl₉]³⁻ are in reassuring agreement with those reported by Bursten *et al.*[12]

(*b*) *Electronic Spectra* (5000–50 000 cm⁻¹).—The Xα-calculated transition energies and calculated oscillator strengths for the octahedral monomers are collected in Table 2 and the corresponding data for confacial bioctahedra in Table 3. In both cases transitions listed in the lower parts are classified as charge transfer in nature. The transitions of [Ru₂X₉]³⁻ of negligible predicted intensity or significance are generally omitted from the band-numbering scheme (see below).

Table 2 Xα-Calculated transition energies (cm⁻¹) and oscillator strengths, *f*, for [RuX₆]³⁻ and [IrX₆]²⁻

	[RuCl₆]³⁻			[RuBr₆]³⁻		
Transition	E_{calc}	*f*	E_{obs}	E_{calc}	*f*	E_{obs}
2t₂g ⟶ 3eg	18 900	0.000		18 200	0.000	
1t₁g ⟶ 2t₂g	18 500	0.000	26 000	12 390	0.000	20 400
3t₁u ⟶ 2t₂g	20 600	0.041	28 200	14 500	0.041	22 500
1t₂u ⟶ 2t₂g	22 800	0.068	31 000	17 000	0.065	25 300
2t₁u ⟶ 2t₂g	29 600	0.021		24 300	0.023	
3t₁u ⟶ 3eg	37 300	0.323	41 800	30 600	0.347	37 000
1t₂u ⟶ 3eg	39 400	0.001		33 100	0.001	
2t₁u ⟶ 3eg	46 400	0.292		40 500	0.337	

	[IrCl₆]²⁻			[IrBr₆]²⁻		
Transition	E_{calc}	*f*	E_{obs}	E_{calc}	*f*	E_{obs}
2t₂g ⟶ 3eg	25 000	0.000		21 200	0.000	
1t₁g ⟶ 2t₂g	9 900	0.000	17 300	4 600	0.000	12 500
3t₁u ⟶ 2t₂g	12 500	0.022	20 400	7 000	0.010	14 600
1t₂u ⟶ 2t₂g	14 500	0.069	23 500	9 000	0.052	17 800
2t₁u ⟶ 2t₂g	22 500	0.040		17 100	0.037	
3t₁u ⟶ 3eg	36 300	0.361	42 000	27 200	0.316	35 800
1t₂u ⟶ 3eg	38 200	0.001		29 100	0.001	
2t₁u ⟶ 3eg	46 400	0.353		37 400	0.400	

Table 3 Xα-Calculated transition energies (cm⁻¹) and oscillator strengths for [Ru₂X₉]³⁻

		[Ru₂Cl₉]³⁻		[Ru₂Br₉]³⁻	
	Transition	E_{calc}	*f*	E_{calc}	*f*
1	6e″ ⟶ 5a₂″	6 200	0.068	5 300	0.057
2	6a₁′ ⟶ 5a₂″	12 300	0.329	9 400	0.252
	6e″ ⟶ 7e″	16 600	0.000	15 800	0.000
	8e′ ⟶ 7e″	17 200	0.003	15 700	0.004
	6e″ ⟶ 9e′	21 200	0.001	20 500	0.004
	8e′ ⟶ 9e′	21 800	0.000	20 400	0.000
3	6a₁′ ⟶ 9e′	26 900	0.016	24 100	0.022
4	5e″ ⟶ 5a₂″	19 900	0.007	13 800	0.004
5	4e″ ⟶ 5a₂″	27 100	0.049	19 600	0.037
6	5e″ ⟶ 7e″	28 700	0.015	22 800	0.014
	7e′ ⟶ 7e″	29 700	0.000	23 800	0.000
7	5a₁′ ⟶ 5a₂″	30 100	0.017	24 600	0.039
	1a₁″ ⟶ 7e″	30 100	0.000	24 200	0.000
8	4a₂″ ⟶ 7e″	30 400	0.142	24 100	0.138
	4a₁′ ⟶ 5a₂″	32 000	0.003	26 200	0.004
9	6e′ ⟶ 7e″	33 000	0.089	26 700	0.090
	2a₂′ ⟶ 9e′	33 100	0.000	27 300	0.002
10	5e″ ⟶ 9e′	33 400	0.054	27 500	0.059
	7e′ ⟶ 9e′	34 300	0.000	28 500	0.000
	3e″ ⟶ 5a₂″	34 400	0.003	28 300	0.001
11	4e″ ⟶ 7e″	36 100	0.042	30 500	0.046
12	6e′ ⟶ 9e′	37 500	0.057	31 400	0.062
13	5e′ ⟶ 7e″	38 300	0.253	32 700	0.283
14	4e″ ⟶ 9e′	40 700	0.061	35 200	0.071
15	2e″ ⟶ 5a₂″	41 900	0.036	36 200	0.053
16	3a₂″ ⟶ 7e″	42 400	0.123	37 800	0.107
	1a₂′ ⟶ 9e′	42 800	0.002	36 900	0.000
17	5e′ ⟶ 9e′	42 900	0.093	37 500	0.094
18	3e″ ⟶ 7e″	43 500	0.113	36 700	0.117

Discussion

(*a*) *x.m.c.t. Spectra of Octahedral Systems*, [MX₆]ᶻ⁻.—The charge-transfer spectra of the numerous d-block [MX₆]ᶻ⁻ complexes (Mⁿ⁺{X₆⁶⁻}) are well described in terms of a simple one-electron promotion model,[17] whereby the excited states are represented by (M⁽ⁿ⁻¹⁾⁺{X₆⁵⁻}). For low-spin d⁵ ions, charge transfer to the LUMO (lowest unoccupied molecular orbital) generates the unique closed-shell t₂g⁶ configuration

[equation (1)] coupled to a one-electron hole on the six-halide

$$[Ru^{III}\{X_6\}^{6-}]^{3-} \xrightarrow{h\nu} [Ru^{II}\{X_6^{\bullet}\}^{5-}]^{3-} \qquad (1)$$
$$(t_{2g}^{5}) \qquad\qquad (t_{2g}^{6})$$
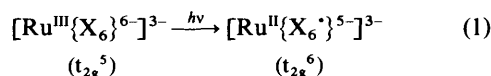
array. The observed spectra then simply map the energies of relevant ligand symmetry orbitals.

The $X\alpha$ calculation generally provides only a weighted average of the energies of all the states arising for a particular configuration rather than locating the most stable component. However, in the case of $X \longrightarrow t_{2g}$ processes in low-spin d^5 complexes, the computed energy corresponds directly with the unique $^1A_{1g}$ state associated with the c.t.-generated t_{2g}^{6} central-ion configuration. In consequence, octahedral complexes with ground-state t_{2g}^{5} populations have the simplest low-energy l.m.c.t. manifolds and also provide the most straightforward test of the $X\alpha$ model.

The UV/VIS spectra of the tervalent hexachlorides, measured in CH_2Cl_2 solution, are characterised by a leading envelope of three bands approximately 2000 cm^{-1} apart, with the lowest-energy band noticeably weaker than the other two. These three bands have been unequivocally assigned to the $1t_{1g} \longrightarrow 2t_{2g}$ (forbidden), $3t_{1u} \longrightarrow 2t_{2g}$, and $1t_{2u} \longrightarrow 2t_{2g}$ transitions respectively,[17a-d] corresponding to promotion from the three upper-most ligand-based symmetry orbitals (see Fig. 2). These levels, together with lower-lying $1t_{2g}$, contain the aggregate of twelve lone pairs of π symmetry on the six halide ligands. Congruent, highly characteristic charge-transfer envelopes are found for all accessible $4d^5$ and $5d^5$ $[MCl_6]^{z-}$ and $[MBr_6]^{z-}$ complexes. The hexabromide visible spectra appear more complicated, due to the emergence of halide-induced spin-orbit multiplets based on the same transitions. The detailed assignments of Dickinson et al.[17g] were used to derive the approximate barycentres of the overlapping $[MBr_6]^{z-}$ multiplets as summarised in Table 2. Well beyond the $X \longrightarrow 2t_{2g}$ envelope lies the more intense and relatively broad absorption band due to charge transfer into the vacant e_g level, specifically assigned as $3t_{1u} \longrightarrow 3e_g$. The optical window between the two band systems is approximately 14 000 cm^{-1} in tervalent $[RuX_6]^{3-}$ ($X = Cl$ or Br). The ratio of measured absorption coefficients for the three strong bands $3t_{1u} \longrightarrow 2t_{2g}$, $1t_{2u} \longrightarrow 2t_{2g}$ and $3t_{1u} \longrightarrow 3e_g$ is approximately $1:1:8$,[17a] for both $[RuCl_6]^{3-}$ and $[IrCl_6]^{2-}$. The absence of an observable $1t_{2u} \longrightarrow 3e_g$ transition will be explained below, in the discussion of oscillator strengths. For the four d^5 complexes $[RuCl_6]^{3-}$, $[RuBr_6]^{3-}$, $[IrCl_6]^{2-}$ and $[IrBr_6]^{2-}$ the calculated $X \rightarrow M$ c.t. energies for these three bands are listed in Table 2 and the experimentally observed values are plotted against the calculated energies (twelve data points in all) in Fig. 3.

Fig. 3 establishes quite dramatically that $X\alpha$-calculated c.t. energies are faithfully linearly related (with unity gradient) to the observed band frequencies. Note that the line shown has been least-squares fitted to the $X \longrightarrow 2t_{2g}$ data only, the subset where the most rigorous test can be made as explained above. Clearly the $X\alpha$ method provides an accurate description of the *relative* energies of x.m.c.t. transitions, but in this case consistently underestimates the absolute x.m.c.t. energies by approximately 8000 cm^{-1}. The relationship is notably conserved over changes in halide (Cl vs. Br), metal (4d vs. 5d), and oxidation state (M^{III} vs. M^{IV}), and approximately embraces the $X \longrightarrow 3e_g$ data as well.

Several factors might affect the inherent underestimation of x.m.c.t. transition energies described above, most notably the spin-orbit splitting of the $^2T_{2g}$ ground state into E_g'' and U_g' states. In $[IrX_6]^{2-}$, for example,[17g] these are separated by as much as 5000 cm^{-1}, so that the weighted mean accessible to $X\alpha$ calculation lies 3300 cm^{-1} above the true ground state. More generally, the disagreement between experimental and calculated energies should depend on the degree of charge transferred (for example, $3e_g$ has greater ligand character than has $2t_{2g}$, so the important $X \longrightarrow 3e_g$ transitions contain a smaller c.t.
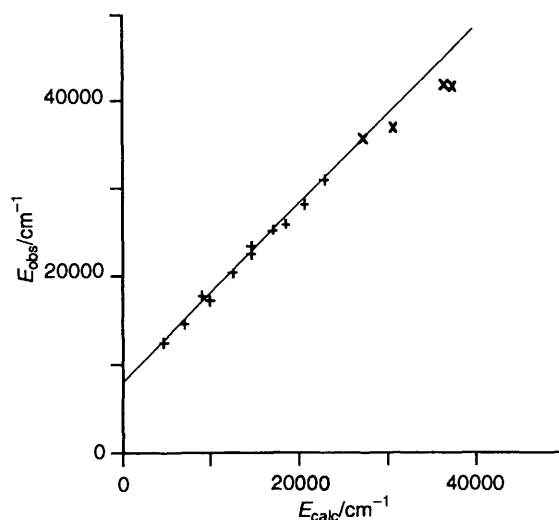
Fig. 3 Correlation of calculated and observed x.m.c.t. energies for d^5 $[MX_6]^{z-}$ monomers. Data from Table 2. The least-squares best-fit line ($E_{obs} = aE_{calc} + c$; $X \longrightarrow 2t_{2g}$ data only) has $a = 1.002$, $c = 7990$ cm^{-1}, and correlation coefficient, $r = 0.996$. +, $X \longrightarrow 2t_{2g}$; ×, $X \longrightarrow 3e_g$

component than do their $X \longrightarrow 2t_{2g}$ counterparts). In fact, the plot of measured vs. calculated $X \longrightarrow 3e_g$ maxima for a wider range of 4d and 5d $[MCl_6]^{z-}$ complexes ($M^{III} = Ru$ or Rh; $M^{IV} = Pd$, Os, Ir or Pt) reveals a parallel linear response with an intercept of 7150 cm^{-1} (gradient 0.99, $r^2 = 0.998$).[28] Obviously, the computed energies also depend significantly on the fidelity of the input geometry.† With these uncertainties in mind we are content to propose that a correction of 7000–8000 cm^{-1} should be anticipated for typical x.m.c.t. transitions. It should be stressed that our subsequent conclusions are unaffected by uncertainties of 1000 cm^{-1} or so in the correction factor. For consistency, a fixed correction ($\delta_{c.t.}$) of 7500 cm^{-1} is applied without equivocation throughout the present work.

With respect to band intensities, it has been shown that the oscillator strengths of x.m.c.t. transitions are largely determined by the overlap of ligand-based components in the molecular donor and acceptor orbitals.[29] In the present context the relevant donor orbitals prove to be essentially purely ligand-based (computed as $\leqslant 5\%$ metal character and $\approx 85\%$ halide character, cf. SUP 57043), so the magnitude of the overlap should be determined by two factors, the amount of ligand character in the acceptor orbital and the mutual physical orientation of the ligand-based components of the donor and acceptor molecular orbitals. This optimum overlap requires that ligand components of π symmetry within the donor orbital find a match with similarly disposed ligand π components in the acceptor orbital, and likewise σ components with σ. The spatial matching of ligand- and metal-centred orbitals in intense c.t. transitions, which we recently illustrated at length,[30] is a corollary of this underlying requirement for optimum overlap of ligand components within the two molecular orbitals.

Contour plots of the metal-centred $2t_{2g}$ and $3e_g$ acceptor orbitals of $[RuCl_6]^{3-}$ are shown in Fig. 4. Two factors foreshadowed above are worthy of note, and will be adopted as principles in subsequent discussion. First, $3e_g$ has considerably greater ligand character than $2t_{2g}$ (40 vs. 20%, for $[RuCl_6]^{3-}$) and consequently x.m.c.t. transitions into $3e_g$ are usually more

---

† For example, two different crystal structures have been reported for $[IrBr_6]^{2-}$, with Ir–Br bond lengths of 2.515(1) and 2.549(3) Å.[24] The structure in solution is undetermined, but an uncertainty in the Ir–Br bond length of 0.03 Å can make differences of up to 1500 cm^{-1} in calculated c.t. transition energies ($X \longrightarrow 3e_g$ transitions are particularly sensitive).

2t$_{2g}$ 3e$_g$

71% Ru, 21% Cl   52% Ru, 40% Cl
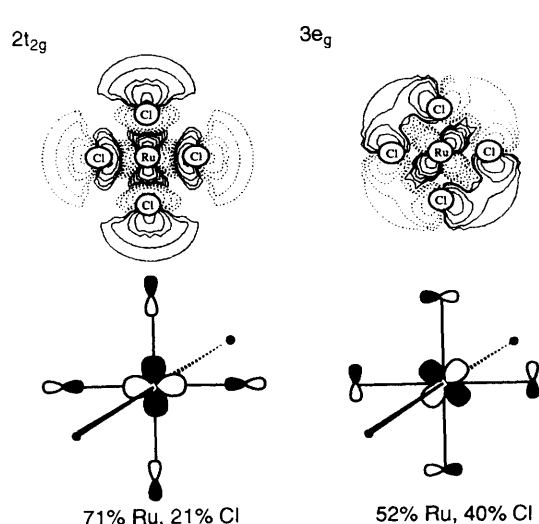
Fig. 4 Contour plots of the 2t$_{2g}$ and 3e$_g$ (c.t. acceptor) orbitals of [RuCl$_6$]$^{3-}$

1t$_{2u}$ 3t$_{1u}$

85% Cl   3% Ru, 84% Cl

Fig. 5 Contour plots of the 1t$_{2u}$ and 3t$_{1u}$ (c.t. donor) orbitals of [RuCl$_6$]$^{3-}$

intense than those into 2t$_{2g}$. Secondly, these molecular orbitals differ in their M–X interaction in that 3e$_g$ is σ* in nature while 2t$_{2g}$ shows π* character. The prospective donor orbitals are shown in Fig. 5; both are roughly 85% halide, but 1t$_{2u}$ is exclusively of π symmetry (henceforth represented X π) while 3t$_{1u}$ has mixed π and σ character (represented X π/σ).

We therefore anticipate an intense transition from 1t$_{2u}$ (X π) into 2t$_{2g}$ (M–X π*) but not into 3e$_g$ (M–X σ*), while 3t$_{1u}$ (X π/σ) should give relatively intense transitions into both 2t$_{2g}$ and 3e$_g$. The oscillator strengths calculated within the SCF-Xα-SW approximation show pleasing agreement with these qualitative expectations. Most notably, the high oscillator strength of the X π/σ→M–X σ* transition (3t$_{1u}$ ⟶ 3e$_g$) compared to that computed for X π/σ→M–X π* (3t$_{1u}$ ⟶ 2t$_{2g}$) is consistent with the higher halide character of 3e$_g$ (the first factor mentioned above), while the negligible oscillator strength of the fully allowed X π→M–X σ* transition (1t$_{2u}$ ⟶ 3e$_g$) indicates the decisive importance of the relative orientation of ligand components in the donor and acceptor molecular orbitals (second factor). For [RuCl$_6$]$^{3-}$ the computed ratio of oscillator strengths for the transitions 3t$_{1u}$ ⟶ 2t$_{2g}$, 1t$_{2u}$ ⟶ 2t$_{2g}$, 3t$_{1u}$ ⟶ 3e$_g$ and 1t$_{2u}$ ⟶ 3e$_g$ is 1 : 1.7 : 8 : 0, in broad accord with the observed ratio of absorption coefficients (1 : 1 : 8, with 1t$_{2u}$ ⟶ 3e$_g$ not detected). In the following discussion the general criterion of matched ligand character in donor and acceptor orbitals will be applied to the more complex problem of interpreting the computed oscillator strengths in confacial bioctahedral systems.

(*b*) *Spectra of Confacial Bioctahedral Systems*, [M$_2$X$_9$]$^{3-}$.— (*i*) *Band positions*. As shown in Fig. 2 the wide separation between the characteristic X ⟶ 3e$_g$ and X ⟶ 2t$_{2g}$ charge-transfer manifolds observed for [RuX$_6$]$^{3-}$ is expected to decrease in moving to [Ru$_2$X$_9$]$^{3-}$. This follows since π* (7e″) is lower than 3e$_g$ and σ* (5a$_2$″) must lie above 2t$_{2g}$, while the terminal halide ligands which should figure prominently in the l.m.c.t. processes are relatively undisturbed by dimerisation. In fact the calculated gap between 5a$_2$″ and 7e″ in [Ru$_2$Cl$_9$]$^{3-}$ is only 10 000 cm^{-1} compared to the 18 000 cm^{-1} between 2t$_{2g}$ and 3e$_g$ in [RuCl$_6$]$^{3-}$.

The electronic absorption spectra of [Ru$_2$Cl$_9$]$^{3-}$ and [Ru$_2$Br$_9$]$^{3-}$, measured in CH$_2$Cl$_2$ solution,[6] are shown in Fig. 6. Predicted transitions numbered as in Table 3 are inscribed as vertical lines with their relative heights scaled to computed oscillator strengths. In the Figure (but *not* the Table) the initial Xα transition energies for frankly charge-transfer processes have been uniformly augmented by 7500 cm^{-1} (δ$_{c.t.}$), as explained above.
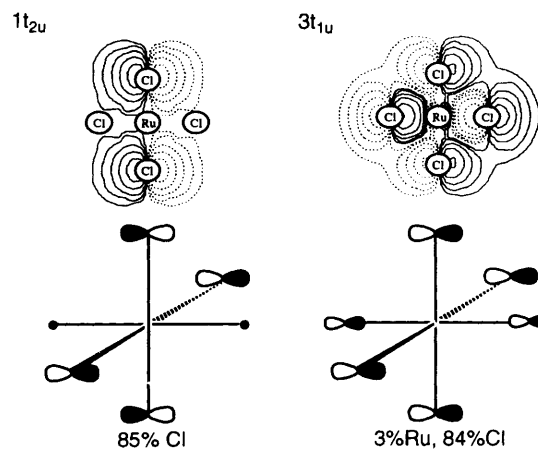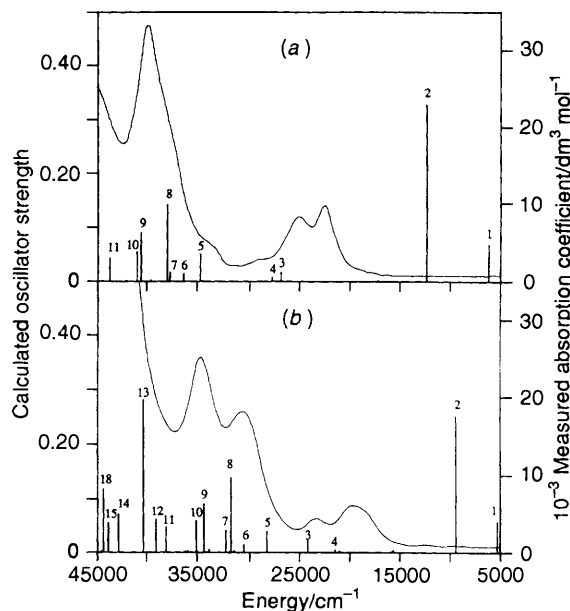
Fig. 6 The UV/VIS spectra of (*a*) [Ru$_2$Cl$_9$]$^{3-}$ and (*b*) [Ru$_2$Br$_9$]$^{3-}$

In the higher ultraviolet region (27 000–45 000 cm^{-1}) [Ru$_2$Cl$_9$]$^{3-}$ has a dominant band at 39 700 cm^{-1} with a pronounced shoulder near 37 000 cm^{-1}, while [Ru$_2$Br$_9$]$^{3-}$ shows distinct bands at 34 800 and 30 600 cm^{-1}. One expects this faithful red shift of about 6000 cm^{-1} between corresponding Cl- and Br-based x.m.c.t. bands, as enshrined in the ligand optical electronegativity scale.[31] These strong absorption bands are readily ascribed to the cluster of transitions numbered from 6 to 10, with transitions 8, 9 and 10 (4a$_2$″ ⟶ 7e″, 6e′ ⟶ 7e″ and 5e″ ⟶ 9e′) being the most important in both complexes. Thus, apart from the minor contribution from transition 7 (5a$_1$′ ⟶ 5a$_2$″), we can conclude that the higher bands are dominated by charge transfer to the {7e″, 9e′} manifold. These absorption bands even resemble their [RuX$_6$]$^{3-}$ 3t$_{1u}$ ⟶ 3e$_g$ counterparts in appearance, though the maxima are red-shifted by several thousand wavenumbers, as foreseen above. Fig. 6 suggests that the double-band system found for [Ru$_2$Br$_9$]$^{3-}$ could be neatly assigned to separate combinations of transitions 6–8 and of 9,10, with the same features simply less well resolved in the spectrum of [Ru$_2$Cl$_9$]$^{3-}$. This may of course be correct, but it should be noted that a similar band structure is observed in the 3t$_{1u}$ ⟶ 3e$_g$ c.t. envelope of monomeric hexabromides where it is tentatively ascribed to halide-based spin–orbit coupling.

With assignment of the intense UV envelope secure, we can turn to consideration of charge transfer into the t$_{2g}$-derived

manifold that is so characteristic of the corresponding monomers. As set out in Table 3, the first such feature should be transition 4 ($5e'' \longrightarrow 5a_2''$) which is expected near 21 000 cm^{-1} for the nonabromide and near 27 000 cm^{-1} for the nonachloride, after incorporation of $\delta_{c.t.}$. Transition 3 is metal-centred rather than charge transfer in nature, which explains the smaller shift between $[Ru_2Br_9]^{3-}$ and $[Ru_2Cl_9]^{3-}$, and will be discussed later. The next $X \longrightarrow 5a_2''$ components (transitions 5 and 7) are calculated to approach or lie within the intense $X \longrightarrow 7e'',9e'$ envelope. As Fig. 6 shows, the prominent near-UV/VIS bands are reasonably placed for a straightforward $X \longrightarrow t_{2g}$-manifold assignment in $[Ru_2Br_9]^{3-}$, but they seem too low in $[Ru_2Cl_9]^{3-}$. Aside from arguments based on absolute frequency, if the near-UV/VIS band envelope contained a dominant x.m.c.t. contribution in both complexes it should be displaced by 6000 cm^{-1} or more between $[Ru_2Br_9]^{3-}$ and $[Ru_2Cl_9]^{3-}$. In fact the shift observed in this envelope is marginal and much less pronounced than the consistent movement associated with authentic $X \longrightarrow 2t_{2g}$ band systems in comparable monomers.

(ii) M_2X_9 Oscillator strength calculations. For more insight regarding the behaviour of the charge-transfer transitions in the binuclear complexes we resort to detailed consideration of band intensities. The oscillator strengths should be ultimately related both to the percentage halide character and to the orientation of these halide components in the relevant donor and acceptor orbitals, as in MX_6. In the trigonal M_2X_9 system the orientation of halide-based symmetry orbitals may be classified as radial, longitudinal or tangential, as illustrated in Fig. 7. The irreducible representations spanned by these sets of ligand orbitals are also shown. Under D_{3h} symmetry, appreciable mixing of radial, longitudinal and tangential character can occur (especially for the terminal ligands, and particularly within the e' and e'' representations), but nevertheless the distinction proves to be useful in interpreting the calculated oscillator strengths. This is because it reflects essentially different modes of M–X bonding, depsite the absence of group-theoretical demarcation. On the terminal ligands, the radially directed atomic orbitals (Fig. 7) correspond to the σ-bonding halide orbitals of the parent monomer, while the longitudinal and tangential atomic orbitals correspond to mutually ortho-gonal π orbitals. This bonding correlation is modified for the bridging halides, where both radial and longitudinal orbitals have mixed σ–π M–X_b character but the tangential orbitals remain approximately pure π.

Fig. 8 illustrates contour plots of the $7e''$ and $9e'$ acceptor orbitals of $[Ru_2Cl_9]^{3-}$, in a plane defined by the Ru–Ru axis, together with one bridging chloride and the two *trans* terminal chloride ligands. These levels, $7e''$ and $9e'$, are of course the acceptor orbitals involved in the intense x.m.c.t. processes, transitions 8–10 and beyond. In $9e'$ the relatively strong antibonding interaction between the Cl_b-based radial p orbitals and the metal-based d orbitals destabilises the molecular orbital sufficiently to outweigh the constructive metal–metal overlap and consequently $7e''$ lies lower than $9e'$, as shown in Fig. 2. These molecular orbitals share high (25–30%) and distinctly radial Cl_t character, but differ in the nature of their 15–20% Cl_b character, which is longitudinal for $7e''$ but radial for $9e'$. According to the criteria established for the hexahalogeno-metalates, intense transitions into both $7e''$ and $9e'$ are anticipated from occupied orbitals with a high degree of radial Cl_t character. Contour plots of the important $4a_2''$ and $6e'$ donor orbitals of $[Ru_2Cl_9]^{3-}$ (with roughly 55% Cl_t character) are shown in Fig. 9.

The $4a_2''$ orbital displays pronounced radial (M–X_σ) quality in its Cl_t components, and consequently, mutual overlap of the Cl_t functions ensures the high computed oscillator strength of transition 8 ($4a_2'' \longrightarrow 7e''$). In addition, $4a_2''$ has 30% Cl_b character which is exclusively longitudinal and matches the similarly disposed Cl_b functions in $7e''$ (see Fig. 8). Thus, the first intense c.t. transition involves a mixture of $X_b \rightarrow Ru$ and
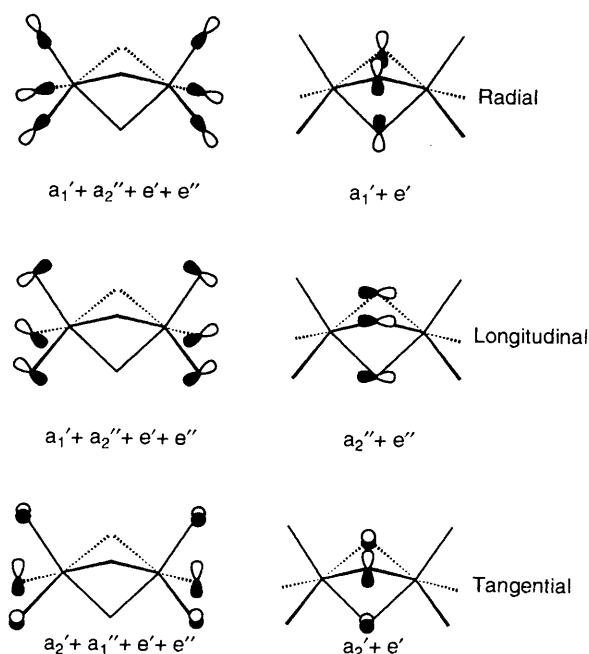
Fig. 7 Classification of halide-based symmetry orbitals in M_2X_9

49% Ru, 15%, Cl_b, 29% Cl_t 49% Ru, 18% Cl_b, 24% Cl_t
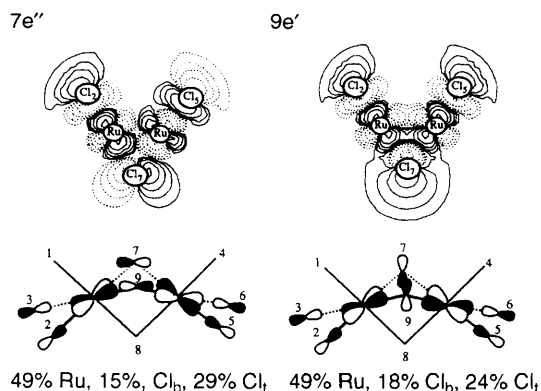
Fig. 8 Contour plots of the $7e''$ and $9e'$ (c.t. acceptor) orbitals of $[Ru_2Cl_9]^{3-}$

3% Ru, 31% Cl_b, 57% Cl_t 8% Ru, 24% Cl_b, 56% Cl_t
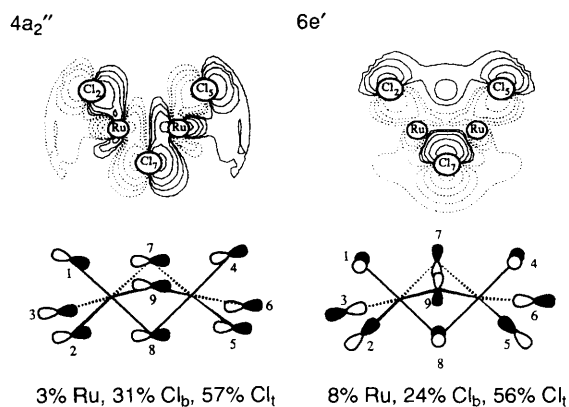
Fig. 9 Contour plots of the $4a_2''$ and $6e'$ (c.t. donor) orbitals of $[Ru_2Cl_9]^{3-}$

$X_t \rightarrow Ru$ charge transfer. The $4a_2'' \longrightarrow 9e'$ permutation is simply forbidden. Like $4a_2''$, the $6e'$ donor orbital has radial Cl_t character which is the primary source of intensity in transitions 9 ($6e' \longrightarrow 7e''$) and 12 ($6e' \longrightarrow 9e'$). Interestingly, transition 9 cannot gain intensity through bridging-halide participation because $6e'$ has zero longitudinal Cl_b character. The same is true of transition 10 ($5e'' \longrightarrow 9e'$) since $5e''$ has zero radial Cl_b

character. In fact, at this level of approximation, the bridging halides do not contribute to the oscillator strengths of any $\phi' \longrightarrow \phi''$ or $\phi'' \longrightarrow \phi'$ transitions where ϕ' and ϕ'' are wave functions symmetric and antisymmetric, respectively, with respect to the σ_h operation in the D_{3h} point group. In summary, on the grounds of mutual orbital orientation as well as energy, it is clear that the $4a_2'' \longrightarrow 7e''$ and $6e' \longrightarrow 7e''$ transitions of $[Ru_2X_9]^{3-}$ (transitions 8 and 9) are closely related to the intense X $\pi/\sigma \rightarrow$ M–X σ^* transitions of the parent octahedron, and make dominant contributions to the UV spectrum. Low-energy allowed transitions to $7e''$ and $9e'$ from $2a_2'$, $7e'$ and $1a_1''$ (occupied orbitals lying higher than $4a_2''$) are related to the X $\pi \rightarrow$ M–X σ^* transitions of $[RuX_6]^{3-}$ (such as $1t_{2u} \longrightarrow 3e_g$) and consequently have vanishingly small oscillator strengths (Table 3).

As already noted, both nonahalides show two moderately intense peaks in the near-UV/VIS region, at approximately 22 500 and 25 500 cm^{-1} for $[Ru_2Cl_9]^{3-}$ and at 19 800 and 23 300 cm^{-1} for $[Ru_2Br_9]^{3-}$, with some evidence of weaker shoulders. Charge transfer into the $\{7e'', 9e'\}$ manifold is unquestionably too high in energy to contribute to these bands, so they must be attributed to X $\longrightarrow$ $5a_2''$ c.t. or internal metal-manifold transitions. Only one calculated charge-transfer excitation, $5e'' \longrightarrow 5a_2''$ (transition 4), falls within the appropriate frequency range (Fig. 6). This excitation is clearly related to the leading X $\pi \rightarrow$ M–X π^* c.t. bands which are prominent for $[MX_6]^{z-}$ monomers (Fig. 1), and so *much rests on the unexpectedly negligible value of the oscillator strength* (0.007) *calculated for the transition*. Fig. 10 shows matching contour plots of $5e''$ and $5a_2''$.

We note that the $5e''$ orbital is almost entirely localised on X_t, and consequently the $5e'' \longrightarrow 5a_2''$ c.t. transition may be classified as relatively pure X_t in origin. The rather small terminal-halide participation in the $5a_2''$ (σ^*) acceptor orbital, only 10% X_t, then predisposes the system to less-intense X $\longrightarrow$ $5a_2''$ c.t. absorption. Moreover, $5a_2''$ necessarily has zero Cl_t tangential character (see Fig. 7) while the Cl_t character of the halide donor level, $5e''$, is partly distributed tangentially. (The tangential character of $5e''$ has a node in the contour plane mapped in Fig. 10, but is shown in the perspective view beneath.) Consequently, inefficient overlap of ligand-based components in the donor and acceptor orbitals leads to a very low computed oscillator strength for the $5e'' \longrightarrow 5a_2''$ transition, and the absorption due to this transition is probably concealed by more intense features. This dramatic loss of $X_t \longrightarrow 5a_2''$ intensity in the visible spectrum, borne out by calculation, is admittedly counter-intuitive. It reflects a situation where confacial dimerisation directs the electron holes into the σ^* orbital which is unfavourably disposed for charge-transfer participation. In effect, dimer formation quenches low-energy $X_t \rightarrow Ru_2(t_{2g})$ charge transfer.

Strong support for this proposition is provided by the optical spectra of the closely related diruthenium(III) complexes $[(H_2O)_3RuCl_3Ru(H_2O)_3]^{3+}$, $[(H_2O)_2ClRuCl_3Ru(H_2O)_3]^{2+}$, and $[(H_2O)_2ClRuCl_3RuCl(H_2O)_2]^{+}$. These are the oxidised forms of Mercer's original triply halide-bridged 'ruthenium blues'.[32] The prominent UV/VIS envelope is remarkably similar for all three complexes and shows no evidence of a contribution from $Cl_t \rightarrow Ru^{III}$ charge transfer accompanying the progressive introduction of terminal chloride ligands. On the contrary, even for $[(H_2O)_3RuCl_3Ru(H_2O)_3]^{3+}$ the envelope has a marked two-component structure, reminiscent of $[Ru_2Cl_9]^{3-}$.

(*iii*) *Metal–metal manifold transitions.* The other $[Ru_2X_9]^{3-}$ transitions computed to lie in the near-UV/VIS region (Table 3) are formally related to the ligand-field splitting in the parent octahedron, in that they connect the t_{2g}- and e_g-based manifolds. Only $6a_1' \longrightarrow 9e'$ (transition 3) has significant calculated oscillator strength. The Xα calculations are known to give reliable estimates of single-ion ligand-field splittings, so we suggest a straightforward connection between the computed

75% Ru, 8% Cl$_b$, 10% Cl$_t$ 1% Ru, 10% Cl$_b$, 79% Cl$_t$
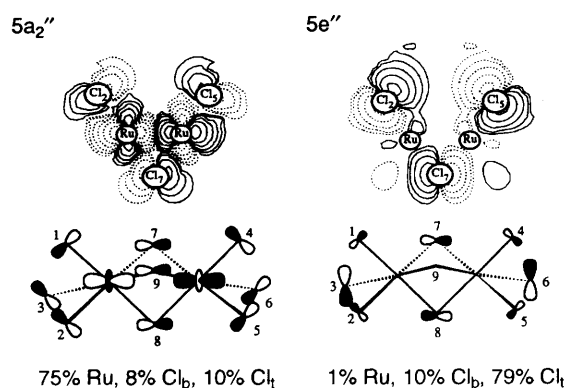
Fig. 10 Contour plots of the $5e''$ (donor) and $5a_2''$ (acceptor) orbitals of $[Ru_2Cl_9]^{3-}$

transition energy and the higher of the two experimentally observed bands: 26 900 *vs.* 25 500 cm^{-1} (observed) for $[Ru_2Cl_9]^{3-}$, and 24 100 *vs.* 23 300 cm^{-1} (observed) for $[Ru_2Br_9]^{3-}$, as in Fig. 6. Support for this assignment comes from the spectra of the $\{d^6d^6\}$ systems, $[Rh_2Cl_9]^{3-}$ and $[Ir_2Cl_9]^{3-}$, where $5a_2''$ is fully occupied and only ligand-field and X $\longrightarrow$ $\{7e'', 9e'\}$ c.t. transitions are possible.[9] Both complexes display prominent bands near 25 000 cm^{-1}, which are appropriately placed for ligand-field type promotions and approximately 10 000 cm^{-1} below the anticipated energy of the first X $\longrightarrow$ $\{7e'', 9e'\}$ band. We conclude that ligand-field related transitions can contribute importantly to the spectra of confacial bioctahedral complexes, where they gain intensity through the lack of an inversion centre.

Returning to $[Ru_2Cl_9]^{3-}$ and $[Ru_2Br_9]^{3-}$, it is clear that the c.t. and ligand-field transitions surveyed above still only account for one strong near-UV/VIS band, *i.e.* transition 3, leaving the other band (most likely, the lower-frequency, more intense of the two) still to be explained. In contrast, the near-IR region is essentially featureless in the experimental spectra, and certainly devoid of strong features. Therefore the anticipated, fully allowed $\sigma \longrightarrow \sigma^*$ transition[2] ($6a_1' \longrightarrow 5a_2''$) must contribute instead to the absorption observed above 20 000 cm^{-1}. This is a secure and consistent assignment, for reasons presented below, even though the Xα-calculated transition energy for $6a_1' \longrightarrow 5a_2''$ is only *ca.* 10 000 cm^{-1}. In this context, it is very significant that an intense band near 12 000 cm^{-1} does emerge upon one-electron reduction of $[Ru_2X_9]^{3-}$ to $[Ru_2X_9]^{4-}$ (X = Cl or Br).[6] This band is similar in energy and appearance to that observed near 14 000 cm^{-1} for the isoelectronic diruthenium(II, III) blues, $[Ru_2X_3(NH_3)_6]^{2+}$, which is unequivocally assigned as the $\sigma \longrightarrow \sigma^*$ transition.[32,33] Thus it appears that the $\sigma \longrightarrow \sigma^*$ transition energy rises by 8000–10 000 cm^{-1} when $\sigma^2\sigma^{*1}$ $[Ru_2X_9]^{4-}$ is oxidised to the $\sigma^2\sigma^{*0}$ state, even though the separation of the relevant orbitals is not much altered.

This striking discrepancy was predictable, at least qualitatively, and is largely due to the strong electron-correlation effects which accompany optical excitation of weakly coupled even-electron states. Consider the anomalous behaviour of the $\delta \longrightarrow \delta^*$ band in multiple-bonded $[Re_2X_8]^{2-}$. Electrogenerated $[Re_2Cl_8]^-$ (+1.5 V) and $[Re_2Cl_8]^{3-}$ (−0.7 V) reveal the $\delta \longrightarrow \delta^*$ band at 6060 and 6950 cm^{-1}, respectively.[34] By interpolation the orbital separation in $[Re_2Cl_8]^{2-}$ should lie close to 6500 cm^{-1}, in impressive agreement with the Xα-computed δ–δ^* orbital separation of roughly 7000 cm^{-1}. The band is actually found near 14 000 cm^{-1} for the dianion. This increase of ≈ 1 eV in transition energy above the independently established δ–δ^* orbital separation may be traced to neglect of electron correlation in Xα wavefunctions. In odd-electron systems, electron-correlation terms effectively cancel out, so the transition occurs close to the calculated orbital separation. As noted in the Introduction, these considerations apply just as much to the configuration-energy relationship between $[Ru_2-$

$X_9]^{3-}$ and $[Ru_2X_9]^{4-}$ as to that between $[Re_2X_8]^{2-}$ and $[Re_2X_8]^{3-}$.

In discussing M_2X_8 $\delta \longrightarrow \delta^*$ transitions, Hopkins *et al.*[18b] established a useful general expression (2) linking the observed

$$hv = (\Delta W^2 + K^2)^{\frac{1}{2}} + K \tag{2}$$

transition energy (hv) to the true energy separation (ΔW) of the one-electron orbitals and an electron-exchange term (K). This treatment is equally appropriate to $\sigma \longrightarrow \sigma^*$ promotion in the confacial bioctahedral systems. In the present study equating hv to the observed band maxima and ΔW to the computed $\sigma \longrightarrow \sigma^*$ orbital energy separation we arrive at K values of 7900 and 7700 cm^{-1} for $[Ru_2Cl_9]^{3-}$ and $[Ru_2Br_9]^{3-}$ respectively.

(*iv*) *Summary of overall* VIS/*near*-UV *spectral assignments.* Accordingly, our assignment of the band system in the visible region for the present complexes is as follows. The peak at 22 500 or 19 800 cm^{-1} for $[Ru_2Cl_9]^{3-}$ and $[Ru_2Br_9]^{3-}$ respectively is assigned to the $6a_1' \longrightarrow 5a_2''$ ($\sigma \longrightarrow \sigma^*$) transition, while the higher band (25 500 or 23 300 cm^{-1}) is assigned to $6a_1' \longrightarrow 9e'$.† The former transition has a calculated oscillator strength ten to twenty times greater and, on this basis, it should dominate the spectrum in this region. However, the intensity of the $6a_1' \longrightarrow 9e'$ absorption may be increased simply by its proximity to $6a_1' \longrightarrow 5a_2''$. Alternatively, the SCF-Xα-SW method may be systematically overestimating the oscillator strengths of the metal-centred processes, $6a_1' \longrightarrow 5a_2''$ and $6e'' \longrightarrow 5a_2''$, leading to unreasonably high predicted intensities for transitions 1 and 2 relative to 3. Features near 15 000 cm^{-1} in the spectra[6] of both $[Ru_2Cl_9]^{3-}$ and $[Ru_2Br_9]^{3-}$ may be due to transition 1. This transition ($\delta_\pi^* \longrightarrow \sigma^*$), like 2 ($\sigma \longrightarrow \sigma^*$), falls within the weakly bonding t_{2g}-derived manifold and electron correlation in the even-electron system should raise the observed transition well above the calculated orbital separation of 6000 cm^{-1}.

Conclusion

In this work we have re-examined well established ideas concerning the electronic absorption spectra of simple MX_6 octahedral systems. We have shown that the same general principles, coupled with detailed Xα calculations, can explain the more complex optical properties of M_2X_9 confacial bioctahedra. This progress relied on establishing an independently determined empirical correction to the halide-to-metal transition energies ($\delta_{c.t.} = 7500$ cm^{-1}). The linear relationship between calculated and observed x.m.c.t. transition energies in monomeric $[MX_6]^{z-}$ complexes has been placed on a very secure footing (spanning X = Cl or Br; M = Ru^{III} or Ir^{IV} for X $\longrightarrow 2t_{2g}$; M = Ru^{III}, Rh^{III}, Pd^{IV}, Os^{IV}, Ir^{IV}, or Pt^{IV} for X $\longrightarrow 3e_g$). The present study also emphasises the need to consider the spatial distribution of the molecular orbitals (rather than merely the net percentage of ligand character) in order to understand the calculated oscillator strengths and observed intensities. The proper interpretation of the UV/VIS spectra of $[Ru_2X_9]^{3-}$ (X = Cl or Br) had previously eluded several authors, including ourselves, and the capacity of theoretically calculated transition energies and oscillator strengths to supplant guesswork by cogent assignments is truly impressive.

---

† It is possible to devise an alternative set of assignments which preserve the naive expectation of prominent x.m.c.t. in the visible region, shifted by 6000–7000 cm^{-1} for replacement of Cl with Br, together with relatively weak ligand-field absorption and the dominant $\sigma \longrightarrow \sigma^*$ absorption: transition 2, 22 500 (Cl), 19 800 (Br); transition 4 (x.m.c.t.) 25 500 (Cl), 18 500(sh) (Br); transition 3, 29 000(sh) (Cl), 23 300 cm^{-1} (Br). However, we conclude that this explanation is already undermined by the qualitative evidence for the aqua species, and by the detailed Xα calculations and will be found wanting by further detailed studies.

In the binuclear $[Ru_2X_9]^{3-}$ complexes intense transitions into the $\{7e'', 9e'\}$ manifold dominate the spectrum above 30 000 cm^{-1}, while the region below 30 000 cm^{-1} is characterised by a combination of ligand-field and metal-manifold transitions. Distinct X $\longrightarrow 5a_2''$ c.t. bands are not observed, as they either have very low intensity (transition 4) or are masked by more intense X $\longrightarrow \{7e'', 9e'\}$ absorption (transitions 5 and 7). Metal-based transitions within the $\{t_{2g}^5, t_{2g}^5\}$ manifold are greatly affected by electron correlation, indicating that these binuclear systems are best described in terms of relatively weak coupling rather than strong covalent bonding. Such correlation effects displace the important $\sigma \longrightarrow \sigma^*$ transition to 20 000–23 000 cm^{-1}, approximately 10 000 cm^{-1} higher than the calculated orbital separation. The resemblance in the optical spectra of $[Ru_2Cl_9]^{3-}$ and $[Ru_2Br_9]^{3-}$ suggests that the metal–metal interactions are similar in the two systems, a conclusion borne out by the calculations. The slightly lower energy of the $\sigma \longrightarrow \sigma^*$ transition in $[Ru_2Br_9]^{3-}$ is a consequence of the longer Ru–Ru bond length imposed by the more bulky bromide ions, rather than a qualitative change in the nature of bonding within the $[MX_3M]^{3+}$ core.

The general picture emerging here has illuminating consequences for a wide variety of related confacial bioctahedral systems. For example, in the oxidised (34-e) form[35] of the ammine-capped ruthenium blues, the presence of terminal aza ligands has two important effects. First, the calculated ligand-field splitting is much larger, displacing the $6a_1' \longrightarrow 9e'$ transition above 35 000 cm^{-1}. Secondly, the characteristic non-participation of the bridging halides, coupled with the absence of π-donor lone pairs on N, means that the low-energy spectrum should be devoid of charge-transfer transitions into $5a_2''$. Consequently, below 30 000 cm^{-1} (*i.e.* below the region of l.m.c.t. to the e_g-derived manifold), the z-polarised $\sigma \longrightarrow \sigma^*$ transition should stand out as the only anticipated strong band. This is borne out by observation since 34-e $[Ru_2Br_3(L)_2]^{3+}$ and $[Ru_2Cl_3(L)_2]^{3+}$ (L = N,N',N''-trimethyl-1,4,7-triazacyclononane) each have a single intense near-UV band, at 24 600 and 26 700 cm^{-1}, respectively.[35] The shift between the bromide and the chloride closely resembles that of 2000 cm^{-1} attributed to the $\sigma \longrightarrow \sigma^*$ band of $[Ru_2Cl_9]^{3-}$ and $[Ru_2Br_9]^{3-}$ which of course have matching $Ru(\mu\text{-}Cl)_3Ru$ and $Ru(\mu\text{-}Br)_3Ru$ cores. Moreover, in the ammine-capped systems, the shift in the $\sigma \longrightarrow \sigma^*$ band between 34- and 35-e forms is again close to 10 000 cm^{-1}. In contrast to the $\{d^5d^5\}$ complexes discussed here, in $\{d^3d^3\}$ $[Mo_2X_9]^{3-}$ and $[Re_2X_9]^-$, 6e'' becomes the lowest unoccupied orbital in the t_{2g}-derived manifold. This has both longitudinal and tangential X_t character and the low-energy spectrum should be dominated by a new family of charge-transfer transitions with appreciable calculated intensity, arising from similarly orientated X_t π-donor orbitals ($X_t \pi \rightarrow M-X_t \pi^*$). In both the dimolybdenum(III) and dirhenium(IV) systems the $\sigma \longrightarrow \sigma^*$ transition is again displaced by 10 000 cm^{-1} or more, and comes to dominate the far-UV region. Our description of these rather different systems will be reported shortly.[28]

The present analysis of $[Ru_2Cl_9]^{3-}$ and $[Ru_2Br_9]^{3-}$ clearly depends on two separate and substantial empirical adjustments to the raw Xα-calculated transition energies, which are adopted in order to make realistic assignments of the x.m.c.t. and $\sigma \longrightarrow \sigma^*$ transitions. In closing we would like to emphasise that these quantitative corrections are far from arbitrary, and indeed they are similar in magnitude to terms known to apply in related systems. Moreover, the major conclusions we have drawn are robust, in that they would not be altered by variations of 1000 cm^{-1} or so in the selected values of $\delta_{c.t.}$ or K. Ongoing improvements in the theory of inorganic electronic structure calculation should eliminate the need for such corrections in due course. The unit relationship between E_{calc} and hv_{obs} for x.m.c.t. transitions, as revealed in the present work, seems a token of this. In the meantime this pragmatic approach offers a workable and fruitful means of making the most of the widely accessible Xα

method, particularly where a significant set of related complexes is available for comparative analysis.

References

1 R. H. Summerville and R. J. Hoffmann, J. Am. Chem. Soc., 1979, 101, 3821; V. T. Coombe, G. A. Heath, T. A. Stephenson and D. K. Vattis, J. Chem. Soc., Dalton Trans., 1983, 2307; W. C. Trogler, Inorg. Chem., 1980, 19, 697; R. Stranger, G. Moran, E. Krausz and G. Medley, Inorg. Chem., 1993, 32, 4555; F. A. Cotton and R. A. Walton, Multiple Bonds between Metal Atoms, Oxford University Press, Oxford, 1993, ch. 9.

2 S. F. Gheller, G. A. Heath, D. C. Hockless, D. G. Humphrey and J. E. McGrady, Inorg. Chem., 1994, 33, 3986.

3 S. F. Gheller, G. A. Heath and D. C. Hockless, unpublished work.

4 P. Hollmann, W. Preetz, H. Hillebracht and G. Thiele, Z. Anorg. Allg. Chem., 1992, 611, 28.

5 (a) A. Broll, H. E. Van Schnering and H. Schäfer, J. Less-Common Met., 1970, 22, 243; (b) E. Babaian-Kibala, F. A. Cotton, L. R. Falvello and M. Shang, Inorg. Chem., 1990, 29, 2591; (c) R. Saillant, R. B. Jackson, W. E. Streib, K. Folling and R. A. D. Wentworth, Inorg. Chem., 1971, 10, 1453; (d) W. H. Watson, jun. and J. Waser, Acta. Crystallogr., 1958, 11, 689; (e) F. A. Cotton, L. R. Falvello, G. N. Mott, R. R. Schrock and L. G. Sturgeoff, Inorg. Chem., 1983, 22, 2621; (f) J. L. Templeton, R. A. Jacobsen and R. E. McCarley, Inorg. Chem., 1977, 16, 3320; (g) P. F. Stokeley, Ph.D. Thesis, Massachusetts Institute of Technology, 1969; (h) J. Darriet, Rev. Chem. Miner., 1981, 18, 27; (i) D. Appleby, P. B. Hitchcock, K. R. Seddon, J. E. Turp, J. A. Zora, C. H. Hussey, J. R. Sanders and T. A. Ryan, J. Chem. Soc., Dalton Trans., 1990, 1879; (j) F. A. Cotton and D. A. Ucko, Inorg. Chim. Acta, 1972, 6, 161.

6 B. J. Kennedy, G. A. Heath and T. J. Khoo, Inorg. Chim. Acta, 1991, 190, 265.

7 G. A. Heath and R. G. Raptis, Inorg. Chem., 1991, 30, 4106.

8 G. A. Heath and D. G. Humphrey, J. Chem. Soc., Chem. Commun., 1990, 672.

9 B. J. Kennedy and G. A. Heath, unpublished work.

10 A. Ginsberg, J. Am. Chem. Soc., 1980, 102, 111; R. J. Ziegler and W. M. Risen, jun., Inorg. Chem., 1972, 11, 2796.

11 F. A. Cotton and R. A. Walton, ref. 1e, p. 605.

12 B. E. Bursten, F. A. Cotton and A. Fang, Inorg. Chem., 1983, 22, 2127.

13 D. A. Case, Ann. Rev. Phys. Chem., 1982, 33, 151.

14 A. Aizman and D. A. Case, Inorg. Chem., 1981, 20, 528.

15 S. J. Desjardins, K. W. Penfield, S. L. Cohen, R. L. Musselman and E. I. Solomon, J. Am. Chem. Soc., 1983, 105, 4590.

16 E. I. Solomon, M. J. Baldwin and M. D. Lowery, Chem. Rev., 1992, 92, 521; A. A. Gewirth, S. L. Cohen, H. J. Schugar and E. I. Solomon, Inorg. Chem., 1987, 26, 1133.

17 (a) C. K. Jorgensen, Mol. Phys., 1959, 2, 309; (b) C. K. Jorgensen, Acta Chem. Scand., 1962, 16, 1048; (c) A. J. McCaffrey, M. D. Rowe and D. A. Rice, J. Chem. Soc., Dalton Trans., 1973, 1605; (d) J. C. Collingwood, P. N. Schatz and P. J. McCarthy, Mol. Phys., 1975, 30, 469; (e) S. B. Piepho, T. E. Lester, A. J. McCaffrey, J. R. Dickinson and P. N. Schatz, Mol. Phys., 1970, 19, 781; (f) S. N. Piepho, J. R. Dickinson, J. A. Spencer and P. N. Schatz, J. Chem. Phys., 1972, 57, 982; (g) J. R. Dickinson, S. B. Piepho, J. A. Spencer and P. N. Schatz, J. Chem. Phys., 1972, 56, 2668.

18 (a) M. B. Hall, Polyhedron, 1987, 6, 696; (b) M. D. Hopkins, H. B. Gray and V. M. Miskowski, Polyhedron, 1987, 6, 705.

19 M. Cook and D. A. Case, Quantum Chemistry Program Exchange, Indiana University, IN, 1982, 4, No. 465.

20 T. E. Hopkins, A. Zalkin, D. H. Templeton and M. G. Adamson, Inorg. Chem., 1969, 8, 2421.

21 M. G. B. Drew, D. A. Rice and C. W. Timewell, Inorg. Nucl. Chem. Lett., 1971, 7, 59.

22 A. J. Lindop, J. Phys. C, 1970, 3, 1984.

23 R. K. Coll, J. E. Fergusson, B. R. Penfold, D. A. Rankin and T. W. Robinson, Inorg. Chim. Acta, 1990, 177, 107.

24 R. E. Watson, Phys. Rev., 1958, 111, 1108.

25 L. Schwarz, Theoret. Chim. Acta, 1974, 34, 225.

26 J. C. Slater, Adv. Quantum Chem., 1972, 6, 1.

27 L. Noodleman, J. Chem. Phys., 1976, 64, 2343.

28 J. E. McGrady, Ph. D. Thesis, The Australian National University, 1994; G. A. Heath and J. E. McGrady, unpublished work.

29 A. van der Avoird and P. Ros, Theoret. Chim. Acta, 1966, 4, 13; E. I. Solomon, Comments Inorg. Chem., 1983, 3, 225.

30 G. A. Heath and C. M. Duff, J. Chem. Soc., Dalton Trans., 1991, 2401.

31 C. K. Jorgensen, Progr. Inorg. Chem., 1970, 12, 101.

32 E. E. Mercer and P. E. Dumas, Inorg. Chem., 1971, 10, 2755.

33 N. S. Hush, J. K. Beattie and V. M. Ellis, Inorg. Chem., 1984, 23, 3339.

34 G. A. Heath and R. G. Raptis, Inorg. Chem., 1991, 30, 4108.

35 D. G. Humphrey, Ph.D. Thesis, The Australian National University, 1992.